Van der Waals interactions and microstructural changes in cellulose microfibrils dispersions

Coen Klik
Studentnumber 3723259
Universiteit Utrecht

June 25, 2014

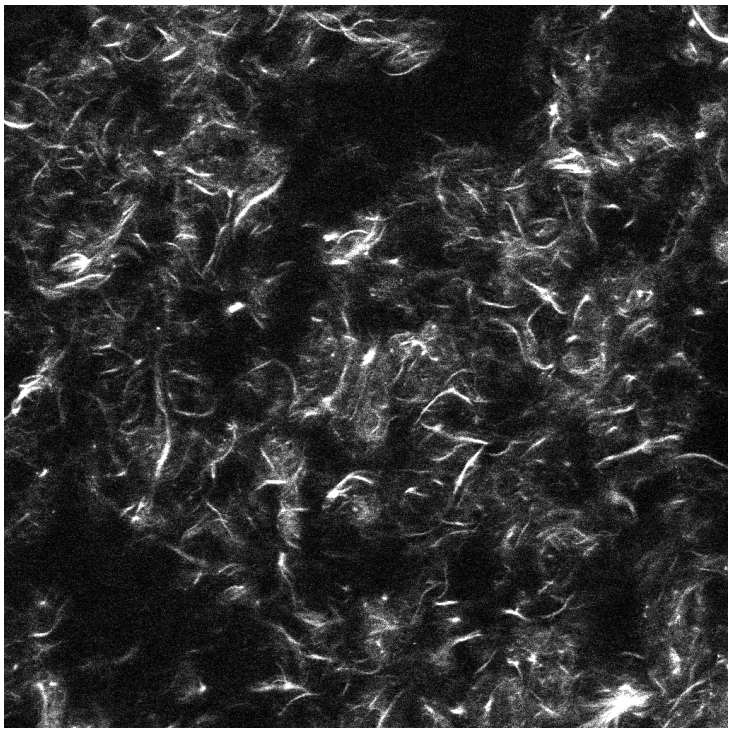

Supervisors: dr. Krassimir P. Velikov, dr. Anke Kuijk, dr. Arnout Imhof
Debye Institute, Soft Condensed Matter

Abstract

Acetobacter xylinum bacteria can use as much as half the energy available to them spinning cellulose fibrils to create a biofilm. The material produced by these bacteria can be deagglomerized, after which the cellulose microfibrils are a good case study of semiflexible fiberlike colloidal particles, which have attracting interactions.

The microfibrils were studied in mixtures of water and glycerol. By measuring the turbidity of microfibril suspensions, the dispersion relation for cellulose was determined, and found to match literature values reasonably well.

The van der Waals free energy was calculated for parallel fibrils in mixtures of glycerol and water. The difference in aggregation caused by the stronger interaction in water and the weaker interaction in glycerol was studied.

By means of transmission spectroscopy and confocal microscopy, microstructural changes due to van der Waals forces were studied. An increase in the turbidity of the samples was measured and attributed to aggregation of microfibrils. In images taken with a confocal microscope, a change of homogeneity of the network of fibrils was observed, when left untouched for several weeks.

It was concluded it is likely the microfibrils were in fact aggregating due to van der Waals interactions over a period of several weeks.

Contents

1 Introduction **3**

2 Theory **4**
2.1 Aggregation of cellulose microfibrils 4
2.1.1 Keesom, Debye and London interaction 4
2.1.2 Van der Waals interaction for macroscopic bodies: the Hamaker constant 5
2.1.3 Molecular structure of cellulose and hydrogen bonds 6
2.1.4 Network structure of cellulose 6
2.2 Refractive index of colloidal particles in turbid suspensions 7
2.2.1 Turbidity 7
2.2.2 Turbidity of a cellulose microfibrils dispersion 8

3 Material and methods **9**
3.1 Cellulose microfibrils dispersions 9
3.2 Spectroscopy 9
3.2.1 Use of the spectrometer 9
3.3 Confocal microscopy 10
3.3.1 FITC, Congo Red 10
3.3.2 Use of the confocal microscope 10

4 Results **11**
4.1 Determination of the refractive index of microfibular cellulose 11
4.1.1 Fitting the turbidity measurements 11
4.1.2 Dispersion relation of cellulose 12
4.2 Turbidity changes of microfibrillar cellulose dispersions 13
4.2.1 Adaptations of methodology after preliminary results 13
4.2.2 Shifts in the transmission spectrum 14
4.2.3 Confocal images of structure 16

5 Conclusion and discussion **19**

Acknowledgements **19**

References **20**

1 Introduction

Cellulose is the most abundant organic polymer on earth. Plants and trees produce it in large quantities, and it is also produced by certain bacteria and algae. The types of cellulose produced by these organisms are structurally different, the one relevant for this thesis is bacterial cellulose, excreted by acetobacter xylinum to form a biofilm.

These bacteria start by spinning the cellulose in so-called protofibrils of around 2 to 4 nm in diameter, [6]. Next they are bundled in a ribbon of 10 to 100 fibrils, which moves the bacterium through the culture, all the while creating a thick gel, see figure 1a.

The fibrils can grow many micrometers long. They are long and thin, and because of van der Waals interaction, the fibrils are attracting, which gives rise to the formation of a network. What the microfibrils look like when deagglomerized can be seen in figure 1b.

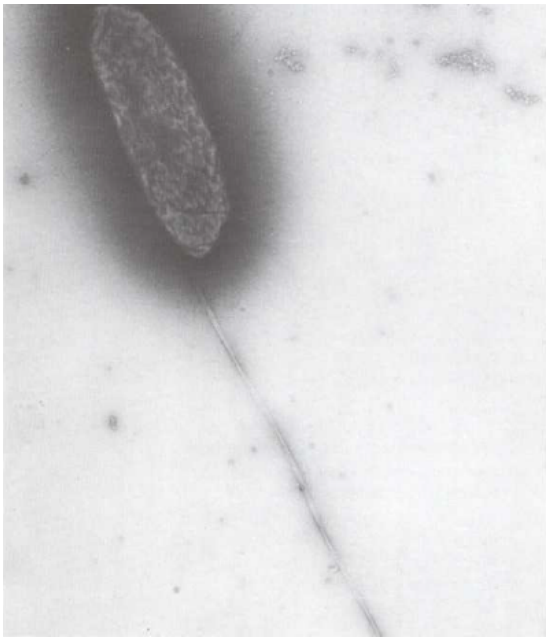

(a) An acetobacter xylinum spinning its ribbon of cellulose microfibrils. [9]

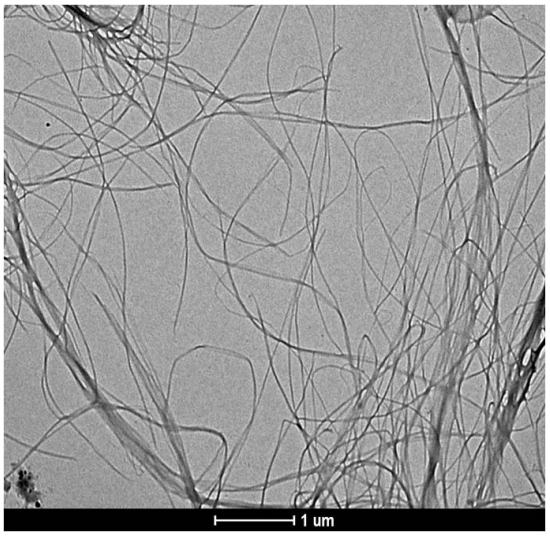

(b) TEM image of microfibrils having been deagglomerized. [8]

Figure 1: Images of bacterial cellulose.

Because the bacteria synthesize pure cellulose, this is a good material to be used to study shape-anisotropic, semiflexible fiberlike particles with attractive interactions, which makes it interesting in and of itself. But microfibrillar cellulose also has many potential applications, in fields such as food, medicine and technology. It can be made into films and sheets which can be used for several purposes such as audio speakers, [6], or even temporary skin for medical care, [2]. It has also been tested to enhance paper, [6]. For use in foods, one can think of using it as an agent to increase the viscosity of a fluid.

In this thesis cellulose microfibrils are studied in water-glycerol mixtures. By measuring the turbidity of the different cellulose dispersions, the refractive index of cellulose is derived. Furthermore changes in the microstructure of the material are studied over time, to see if further aggregation of microfibrils occurs on a timescale of several weeks.

2 Theory

To study the attractive forces between the fibrils, we first need to be aware what are the relevant forces acting on the particles, and what kind of characteristics they have. In the second part of this section the necessary theory for extracting the refractive index of cellulose from turbidity measurements is set out.

2.1 Aggregation of cellulose microfibrils

Cellulose fibrils are electrically neutral. However, there are van der Waals forces between the particles, furthermore cellulose can form hydrogen bonds. We will look at the nature of the van der Waals forces between the fibrils, and see in what way they aggregate.

2.1.1 Keesom, Debye and London interaction

The van der Waals force is the name given to the collection of three intermolecular forces which have a $\frac{1}{r^6}$ force law. Which means that when dealing with molecules, its immediate effects are only on the scale of a molecule's nearest neighbours. To better understand the nature of these three forces, they will be discussed here separately, [4].

The first interaction we discuss is the Keesom interaction, which is the interaction between two permanent dipoles, with dipole moment u_i, a distance r apart. When averaging the dipole-dipole interaction over all orientations, you find a free energy

$$w(r) = -\frac{u_1^2 u_2^2}{3(4\pi\epsilon_0\epsilon)^2 kTr^6}$$

Because of the averaging over orientation, it is also called the orientation interaction.

The second interaction is the Debye interaction, which is when the dipole moment of one molecule, u_i polarizes another molecule with polarizability $\alpha_{0,i}$. The free energy for this interaction is given by

$$w(r) = -\frac{u_1^2\alpha_{0,2} + u_2^2\alpha_{0,1}}{(4\pi\epsilon_0\epsilon)^2 r^6}$$

Because it is an induced dipole interaction, it also referred to as the induction interaction.

The third and most important interaction is the London interaction, which is caused by dispersion. It has its roots in a quantummechanical effect, and can be seen as a dipole interaction of very short duration. It can be related to the first ionization potential of a molecule $I = h\nu$. For two molecules this results in a free energy given by

$$w(r) = -\frac{3}{2}\frac{\alpha_{0,1}\alpha_{0,2}}{(4\pi\epsilon_0\epsilon)^2 r^6}\frac{h\nu_1\nu_2}{\nu_1+\nu_2}$$

This equation has some issues, it uses a single absorption frequency and doesn't account for interaction in a solvent. An improvement is McLachlan's expression for the van der Waals free energy of two molecules across a medium.

$$w(r) = -\frac{6kT}{(4\pi\epsilon_0)^2 r^6}\sum_{n=0}^{\infty}{}' \frac{\alpha_1(i\nu_n)\alpha_2(i\nu_n)}{\epsilon_3^2(i\nu_n)} \tag{1}$$

Here the prime on the summation mark signifies the $n = 0$ term should be multiplied by $\frac{1}{2}$, and α_j is the polarizability of molecule j at imaginary frequency $i\nu_n$ where $\nu_n = \frac{2\pi kT}{h}n$. This energy can be split into a sum of the $\nu = 0$ term, and the ν>0 term. The $\nu = 0$ term turns out to be composed of both the Keesom and the Debye energies.
The microscopic nature of the van der Waals interaction will not be expanded upon further, instead the focus will be on macroscopic bodies.

2.1.2 Van der Waals interaction for macroscopic bodies: the Hamaker constant

After this general introduction into the nature of van der Waals forces between molecules, we will now discuss the potential between two macroscopic bodies. Specifically we would like to discuss the energy of the bond between two solid cylinders. To simplify matters we will focus on the energy of two parallel cylinders, and two perpendicular cylinders, see figure 2.

(a) Two parallel cylinders (b) Two crossed cylinders

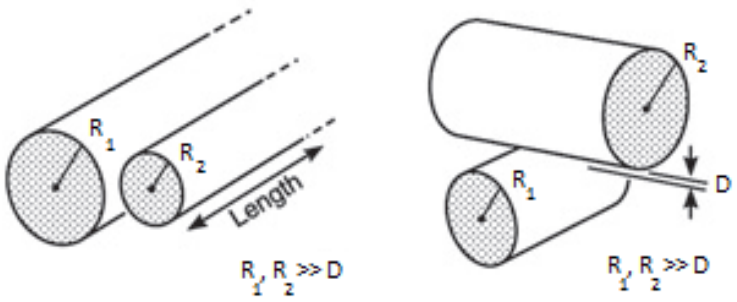

Figure 2: Parallel and crossed cylinders [4]

When dealing with large bodies, the van der Waals energies may be summed over their atoms to find a two-body potential. For cylinders of radii R_1 and R_2, the energy of this interaction for parallel and perpendicular orientations is respectively (see [4])

$$W(D) = \frac{-A}{12\sqrt{2}D^{\frac{3}{2}}}\sqrt{\frac{R_1R_2}{R_1+R_2}} \qquad W(D) = \frac{-A\sqrt{R_1R_2}}{6D} \tag{2}$$

where $D \ll R_1, R_2$ is the distance between the cylinders, and A is the Hamaker constant, which depends on the materials of the cylinders and the medium. Using equation (1), and using Lifshitz theory, an expression can be found for the Hamaker constant in terms of the refractive indices and dielectric constants of the materials.

$$A = \frac{3}{4}kT\frac{\epsilon_1-\epsilon_3}{\epsilon_1+\epsilon_3}\frac{\epsilon_2-\epsilon_3}{\epsilon_2+\epsilon_3} + \frac{3h\nu_e}{8\sqrt{2}}\frac{(n_1^2-n_3^2)(n_2^2-n_3^2)}{\sqrt{n_1^2+n_3^2}\sqrt{n_2^2+n_3^2}(\sqrt{n_1^2+n_3^2}+\sqrt{n_2^2+n_3^2})}$$

Here ν_e is the main electronic absorption frequency, which typically is $3 \times 10^{15}\ \mathrm{s}^{-1}$ [4]. When the cylinders are made of the same material, we can simplify this expression.

$$A = \frac{3}{4}kT\left(\frac{\epsilon_p-\epsilon_s}{\epsilon_p+\epsilon_s}\right)^2 + \frac{3h\nu_e}{16\sqrt{2}}\frac{(n_p^2-n_s^2)^2}{(n_p^2+n_s^2)^{\frac{3}{2}}} \tag{3}$$

where ϵ_p, ϵ_s, n_p, n_s are the dielectric constants and refractive indices of the particle and the medium.

Using equations (2) and (3), the energy of the van der Waals interaction can be plotted to the literature values to illustrate the attracting force between cellulose microfibrils. We used $\epsilon_{water} = 80.1$, $\epsilon_{glycerol} = 46.53$, $\epsilon_{cellulose} = 6$, $n_{water} = 1.3330$, $n_{glycerol} = 1.4735$ and $n_{cellulose} = 1.544$.
For parallel cylinders of radius 30 nm, the resulting energy per micron is plotted in figure 3.

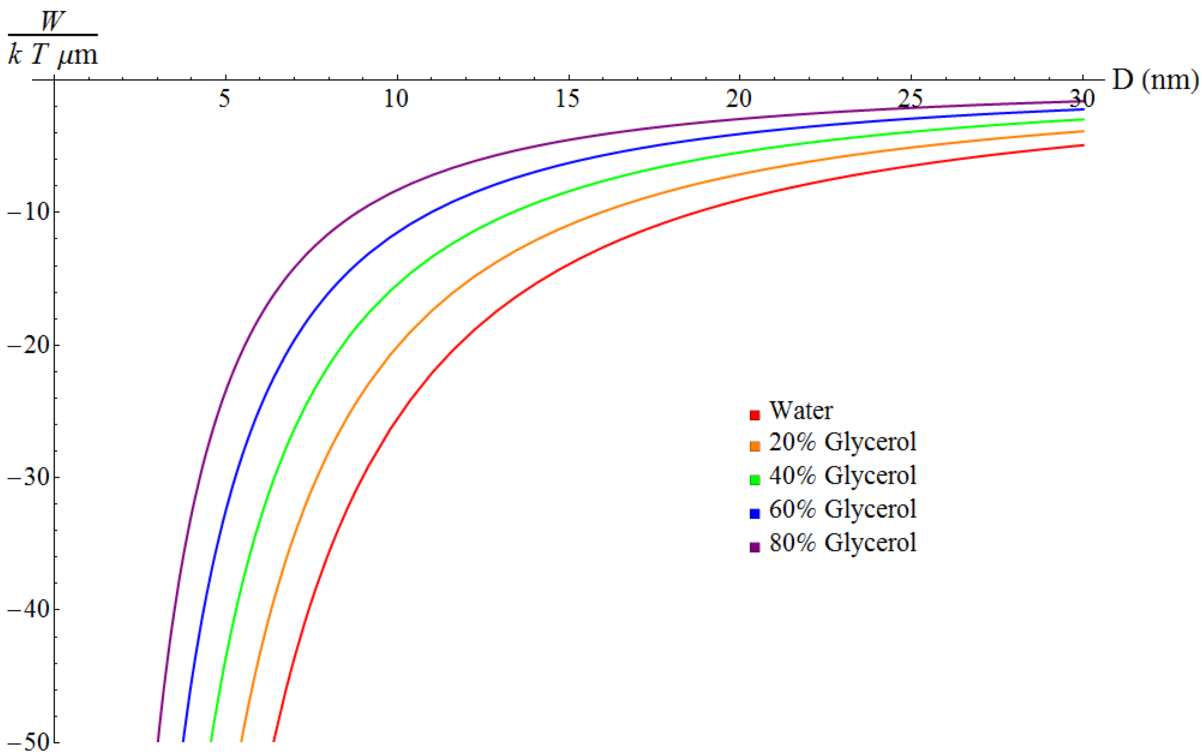

Figure 3: Energy per kT µm of parallel microfibrils at distance D

The van der Waals attraction between these fibers is obviously quite strong, but in solutions with a high glycerol content, though still quite strong, it is significantly weaker. A similar plot can be made for the energy of perpendicular cylinders, but this energy is smaller, only reaching $10kT$ at distances closer than 5 nm for water, and requiring even smaller distances for glycerol-water mixtures.

2.1.3 Molecular structure of cellulose and hydrogen bonds

Cellulose is a polymer made from glycerol. In other sources such as wood, the cellulose often is not very pure, but in bacterial cellulose it is, which makes it an interesting system to examine. To further understand the aggregation of the cellulose microfibrils we take a look at its molecular structure. When we do this, we see it will form hydrogen bonds, see figure 4.

So the microfibrils are held together not only by van der Waals forces, but hydrogen bonds help to strengthen aggregates of fibrils as well.

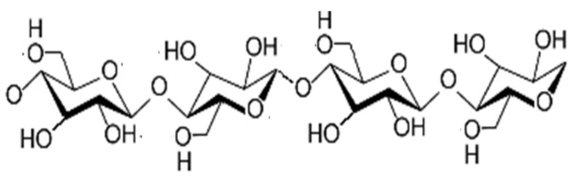

Figure 4: The molecular structure of cellulose

2.1.4 Network structure of cellulose

We have seen there is a strong attraction between cellulose microfibrils, more so in water than in glycerol. Because of this the fibrils tend to line up in large bundles. It is thought this can be explained by the low zeta potential of cellulose [8]. As the microfibrils aggregate, an accumulation of charges forms which stops the growth of aggregate.

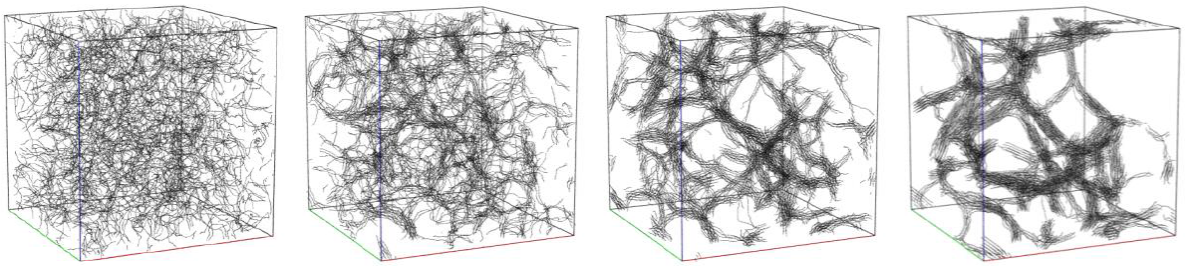

Figure 5: Simulation of network formation [3]

Taking into account the attraction of microfibrils is weaker in solutions of refractive index closer to its own refractive index, such as glycerol, the typical bundle size will be smaller in such solutions than the 15 µm which was found in water.
Furthermore, in water, the cellulose aggregates in flocks, leaving voids of hundreds of µm. When the attractive forces aren't as strong, it is expected the dispersion will be more homogeneous.

2.2 Refractive index of colloidal particles in turbid suspensions

When light passes through a suspension of colloidal particles, scattering occurs. The scattering is affected by the difference in refractive index of the colloidal particles and the medium, as well as the shape and density of the particles. By measuring the turbidity of different samples containing the same particles, but put within a medium of different refractive index, it is therefore possible to determine the refractive index of the particles.

2.2.1 Turbidity

The turbidity, τ, of a solution is a measure of how much light is scattered when it passes through the solution. A solution with $\tau = 0$ doesn't scatter any light, while a solution with turbidity close to 1 barely lets any light through at all. It is often defined as

$$\tau = 2\pi \int_0^\pi \frac{I_\theta}{I_0} \sin\theta \, \mathrm{d}\theta$$

where I_θ is the intensity of light scattered over an angle θ.

The intensity of light passing through a solution of thickness z is described by means of the optical density, D.

$$\frac{I_t}{I_0} = 10^{-Dz}$$

Here I_t is the transmitted intensity, and I_0 is the incident intensity.
Both scattering and absorption may play a role in increasing a solution's optical density. Suppose absorption can be neglected, then

$$I_t = I_0 - I_0\tau \quad \text{or} \quad \tau = 1 - \frac{I_t}{I_0}$$

and thus turbidity can be measured via the transmission intensity, for example by use of a spectrometer in transmission mode.

2.2.2 Turbidity of a cellulose microfibrils dispersion

The turbidity of a solution of randomly oriented long and thin rods is ([5],[10])

$$\tau\lambda^5 = 2\pi^3 C n_s \mu \left(\frac{\mathrm{d}n}{\mathrm{d}c}\right)^2 \frac{44}{15}\left(\lambda^2 - \frac{184}{154}\pi^2 a^2 n_s^2\right) \tag{4}$$

where C is the mass concentration of the rods, n_s is the refractive index of the medium, μ is the mass per length ratio of the rods, $\frac{\mathrm{d}n}{\mathrm{d}c}$ is the specific refractive index increments of the rods, and a is the radius of the rods.
To obtain this equation, several approximations were made [10]. We will discuss their validity in our situation.

The Rayleigh-Gans-Debye approximation, that is, $\frac{n_p}{n_s} \simeq 1$. When we take the literature value for cellulose fibers (in the transverse direction) of 1.544 (for example [1]), 1.333 of water and 1.472 of glycerol, for cellulose in water we find $\frac{1.544}{1.333} = 1.16$, and for 80% glycerol we find $\frac{1.544}{1.445} = 1.07$. So the approximation is valid, but more so for high glycerol solutions.

The wavelength of the light is approximated as being much smaller than the length of the rods, but larger than the average radius. The microfibrils are many micrometers long, so they are easily long enough. On first inspection they are thin enough as well, having an average width of 60 nm, [8]. However, because of bundle formation, we cannot be certain of this, especially when attracting forces between the microfibrils are large, such as in water. In water they are seen to form bundles of 15 µm width [8].

Using equation 4 we will determine the refractive index of the cellulose microfibrils. This is done by fitting this equation to the refractive index of the medium and subsequently finding the root of this equation, that is, where $\tau = 0$, or $\frac{I_t}{I_0} = 1$. The point where this occurs is the point of refractive index matching.

3 Material and methods

3.1 Cellulose microfibrils dispersions

The samples used for the experiments described in this section were performed using 0.17w% cellulose microfibril samples made from a nata de coco source as received from Anke Kuijk, for more information on the extraction of the fibrils from nata de coco pellicles, see [8]. These samples had FITC attached to the cellulose to facilitate confocal microscopy. They had approximate glycerol weight percentages of 0%, 20%, 40%, 60% and 80%. There was some uncertainty in the glycerol content, because of excess fluid in the homogenizer, which cannot be allowed to run dry. Furthermore, because of their high viscosity, due to mixing, there were some air bubbles in the samples with the highest glycerol content.

To remove the air bubbles, which would interfere with the measurements, the samples containing 60% and 80% glycerol were centrifuged slowly, so as to prevent any sedimentation.

To be more certain of the refractive index of the medium, the samples were filtered using a 5 µm SVLP filter. The refractive index of the filtrate was measured using an Abbe type refractrometer. The results are 1.3336, 1.3629, 1.3931, 1.4215 and 1.4460, with an uncertainty of 0.0005, because of temperature effects and inherent uncertainty of the refractrometer. Using these values, samples were made containing the same water-glycerol ratio, to serve as a comparison when using the spectrometer. The refractive indices were less than 0.0005 refractive index units apart, which was sufficiently close for our purposes.

3.2 Spectroscopy

3.2.1 Use of the spectrometer

A HP 8452A Diode Array Spectrophotometer was used in transmission mode. This spectrometer uses 1 cm cuvettes. The transmission spectrum was measured between 190 nm and 820 nm in steps of 2 nm. For each of these points the transmission intensity was measured, including an uncertainty in this intensity. This uncertainty was very small, so other causes of uncertainty such as temperature effects or concentration fluctuations are assumed to dominate the uncertainty of the spectrometer, which is why these uncertainties weren't used in the analysis of the results. It was not possible to measure the lower part of the spectrum, below 300 nm, which has therefore been omitted from the results.

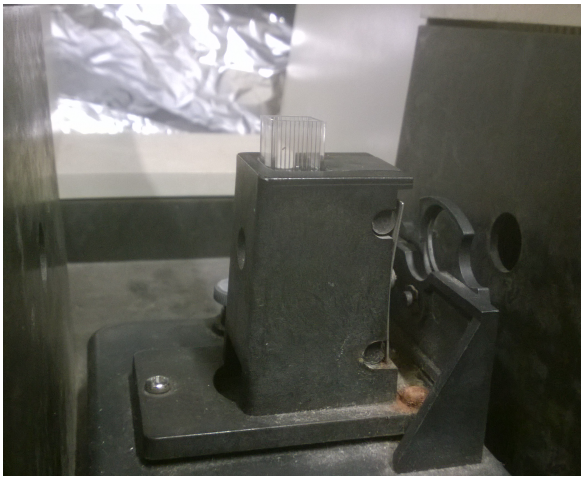

Figure 6: A cuvette in the spectrometer

For each sample, the measurement was repeated three times, to be more certain the measurement was successful.

3.3 Confocal microscopy

A confocal microscope uses lasers to excite a fluorophore in the sample. The excited fluorophore emits light of a higher wavelength. Using lenses, filters and a pinhole, only light from a very specific part of the sample, and of a certain wavelength, is collected into a photomultiplier. By scanning over the sample, each pixel is measured separately, and often many times, to create a complete image.

3.3.1 FITC, Congo Red

For the first images we tried to make of the structure of the cellulose, the chemically bonded fluorescent dye FITC was used. Up until the sample of 40% glycerol this produced good images, however, for the samples of 60% and 80% glycerol the fluorescence was quenched severely, to the point that at maximum laser intensity and PMT gain, only the largest aggregations of cellulose fibrils were vaguely visible, while reflection images showed a lot of cellulose was present. Trying to find the mechanism behind this effect fell outside of the scope of this project, so a different dye was used as a fluorescent: congo red dye. A single drop of 0.5% congo red dye in water was added to 1 mL of sample. Imaging the fibers this way worked well.

3.3.2 Use of the confocal microscope

A Leica TCS SP2 confocal microscope was used, using the preset TRITC settings, and a $20\times$ air objective. The sample was put in an approximately 5 mm thick glass plate with a hole drilled through it, with on each side a coverslip, see figure 7. This way the shear effects, which had been noticed when a drop of the sample was put between two glass plates, were eliminated.

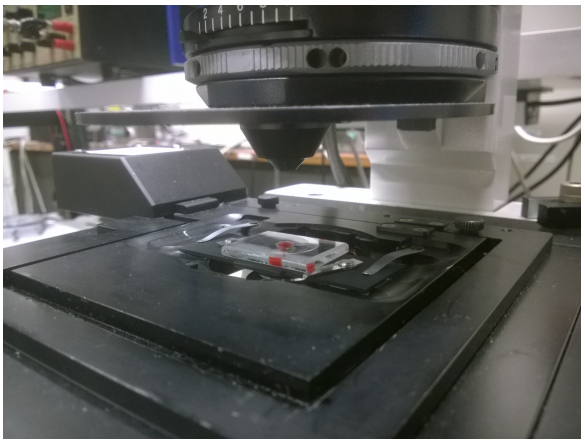

Figure 7: The sample in the microscope

On each sample five different locations were picked approximately 25 µm deep into the sample, and on each of these locations three pictures were made using $1\times$, $2\times$ and $4\times$ zoom, which resulted in images with dimensions of 750×750 µm^2, 375×375 µm^2, and 187.5×187.5 µm^2.
The line and picture averaging was set at a level such that taking another picture to average over did not improve the resulting picture any further, this was mostly $4\times$ line and $3-4\times$ picture averaging.
The laser intensity was set at 86% and the photomultiplier gain was set at 997 V. The offset was set low for samples of high glycerol content, and higher for samples of lower glycerol content, because it was apparent this improved results.

4 Results

4.1 Determination of the refractive index of microfibular cellulose

In section 2.2.2 we discussed the applicability of equation (4) to our system. Using this equation the refractive index of the cellulose microfibrils will be extracted from the spectroscopy measurements. A typical transmission spectrum of the cellulose microfibrils samples can be seen in figure 8.

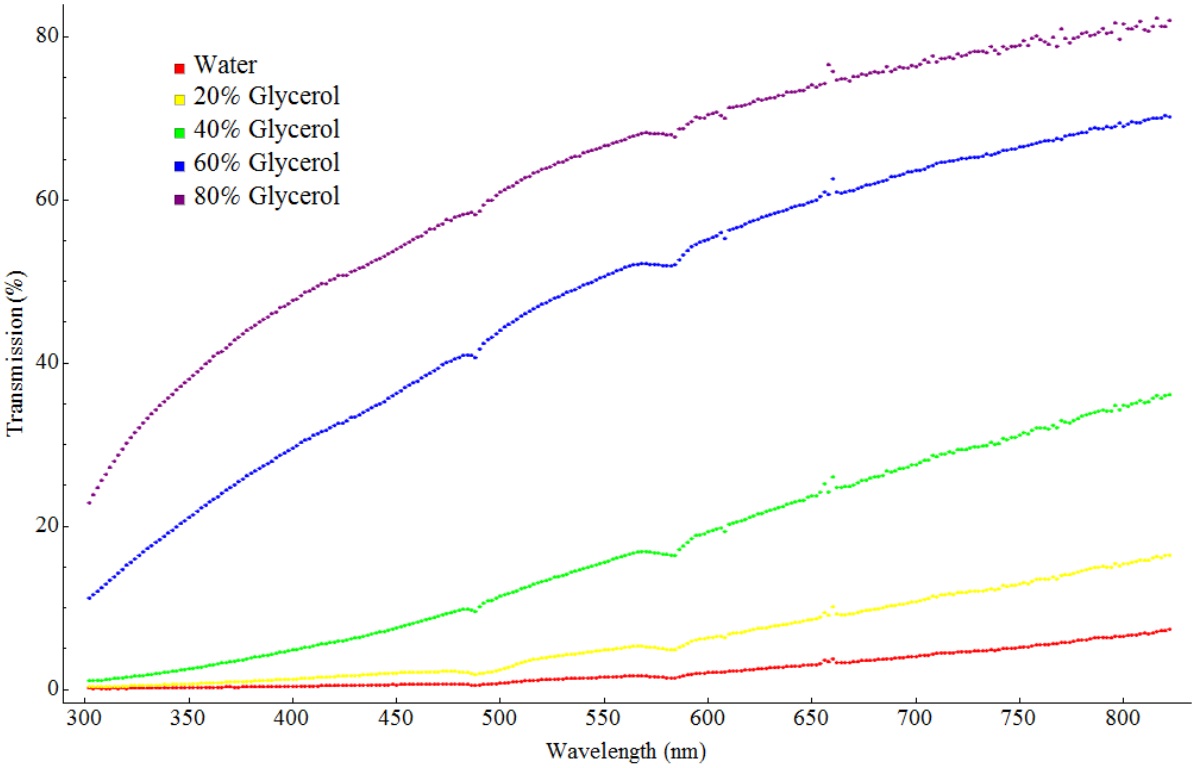

Figure 8: A typical transmission spectrum of cellulose microfibrils in media of different refractive indices

4.1.1 Fitting the turbidity measurements

From the transmission spectra of the different samples, the turbidity can be fitted for several wavelengths. To do this we rearranged equation (4):

$$\tau = \frac{88}{15}\frac{\pi^3}{\lambda^3}C\mu\frac{\mathrm{d}n}{\mathrm{d}c}^2(n_s - \frac{92\pi^2}{77}\frac{a^2}{\lambda^2}n_s^3) = A(n_s - \frac{B^2}{\lambda^2}n_s^3) \tag{5}$$

Here A and B are fitting parameters. The samples containing only a low fraction of glycerol are much more turbid than the ones with a high fraction of glycerol, as is to be expected. Because of the different structure of the network of fibrils, and the mismatch with the other samples, the measurements of the water sample have been omitted from this fit, for small wavelengths this was done for the 20% glycerol sample as well. Whether the 20% glycerol point was omitted from the results depended on whether this affected the uncertainty in the fit parameters positively or negatively.
This is further supported by the knowledge that transmission measurements are less trustworthy at transmission intensities below and close to 1%.

The fitted turbidity curves are shown in figure 9.

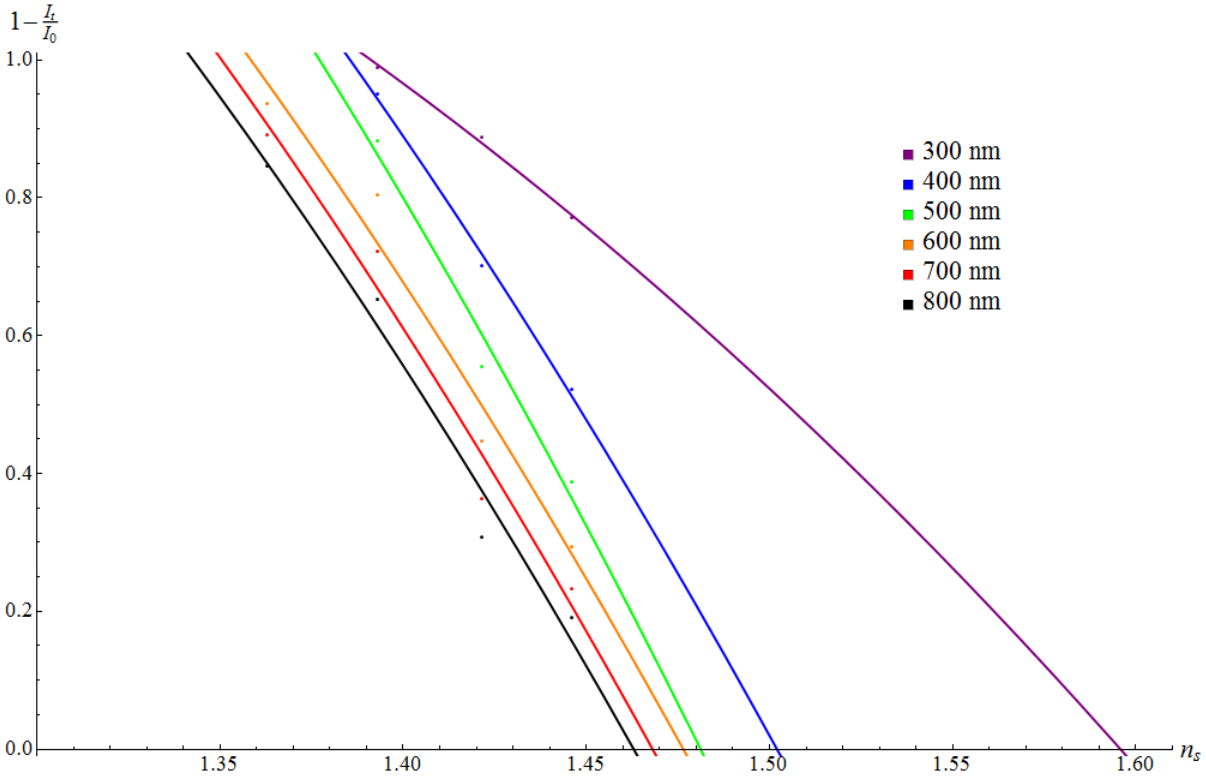

Figure 9: Fit of the turbidity of cellulose microfibrils dispersions at several wavelengths

4.1.2 Dispersion relation of cellulose

From the value of parameter B in equation 5 we know the root of the expression, which is the measured turbidity.
Now that we have extracted the refractive indices of cellulose for several wavelengths, it is interesting to look at the dispersion relation. In figure 10 the measured refractive indices have been plotted with the dispersion relation found in literature, [7]. It is clearly not a perfect match, but especially for higher wavelengths the measurements match the literature quite well.

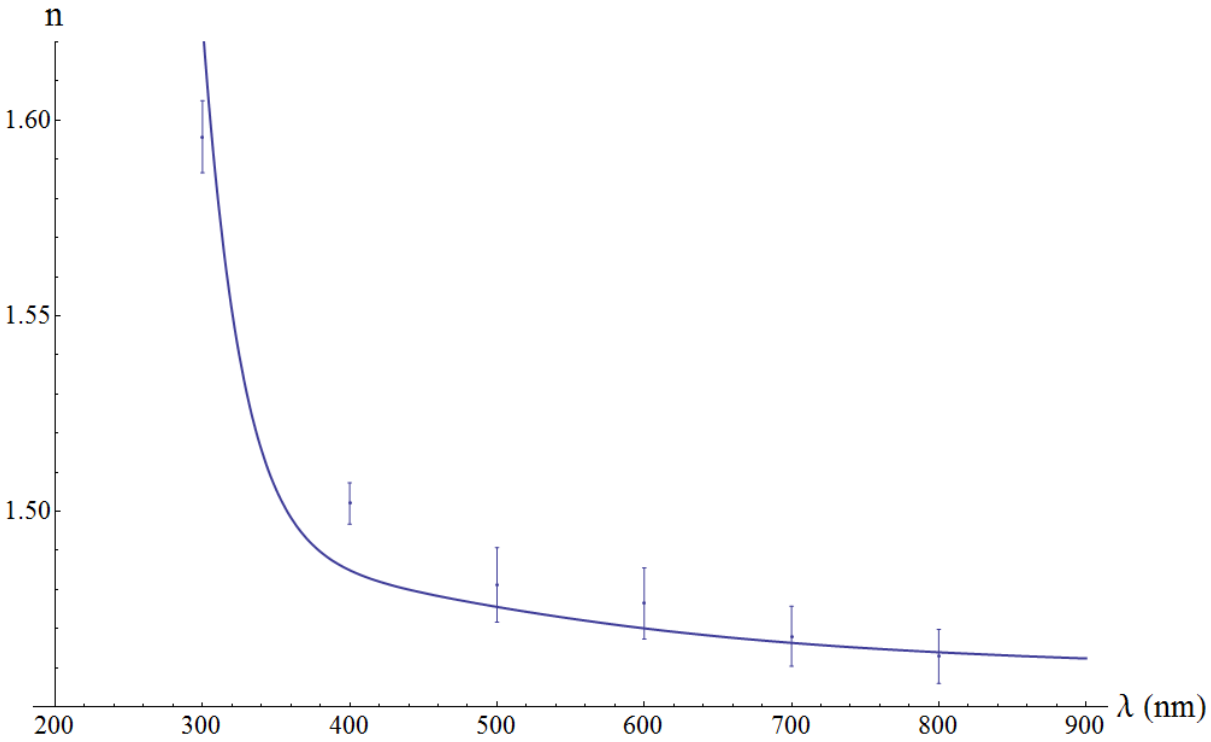

Figure 10: Measured refractive indices and the dispersion relation from literature.

4.2 Turbidity changes of microfibrillar cellulose dispersions

In an older sample, a change in turbidity was noticed when left untouched for several months. To be able to quantify this change, spectroscopy measurements were repeated over a period of several weeks.

4.2.1 Adaptations of methodology after preliminary results

It should be noted that while the samples were prepared on March 19th, and brought to Utrecht on March 21st the first spectroscopy measurements were only made on April 2nd. So any structural processes occurring in the first two weeks have not been measured. Furthermore, over the course of the experiment, the procedure for measurement was refined to rule out possible causes of uncertainty. The weeks will be numbered starting with the week of 24 March as week 1

In week 2, measurements were done on samples which had all been centrifuged, some to the point that sedimentation had occurred. Of course they were mixed afterwards, but this harsh centrifuging likely had an effect on the aggregation of the cellulose fibers, so a new set of sample bottles were made and centrifuged when necessary, this time more slowly so as to prevent sedimentation. Measurements on the old set continued side by side with the new set.

In subsequent weeks the spectroscopy measurement was done in new cuvettes each time. After examination of the first results, which were not showing an obvious pattern, from week 5 onward the sample was kept in the same cuvettes to rule out any uncertainty caused by inhomogeneities in the bottle, even though these should be minimal, since the bottles have been mixed for a substantial amount of time.

Because these changes in method might have an effect, it is good to keep them in mind when examining the results.

4.2.2 Shifts in the transmission spectrum

The results of the spectroscopy measurements will be split into two sections, up to week 6, and from week 6 onward. By separating these results, it will be easier to see the pattern found in the second part.

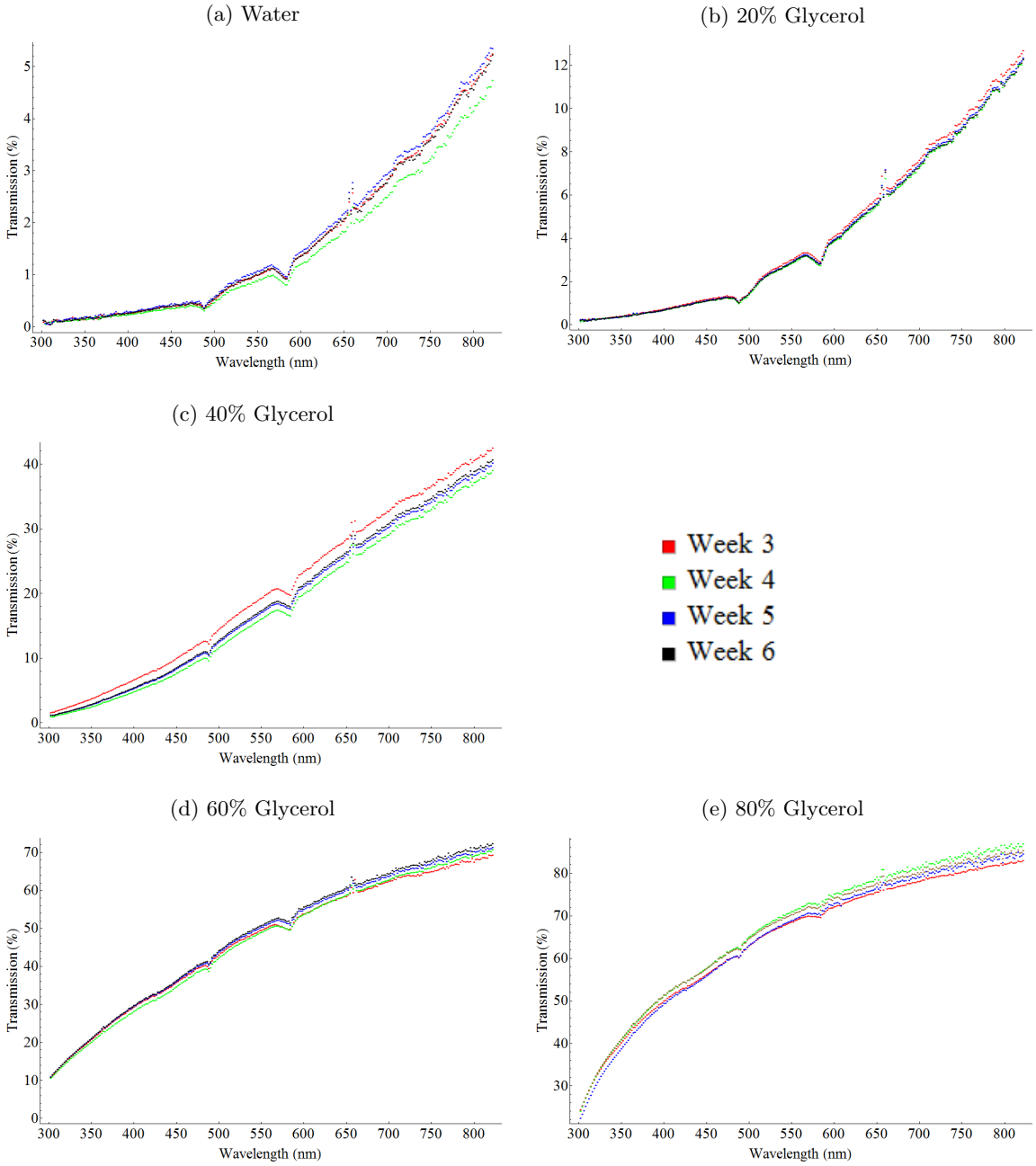

Figure 11: Spectroscopy measurements in week 3 to week 6

When examining figure 11 there is no obvious trend, we see neither a trend of increasing or decreasing turbidity for a single sample, nor do we see a similar pattern over and over in each sample. This might support the idea there isn't any significant aggregation happening, with measured differences in turbidity merely appearing due to inhomogeneities in the sample.

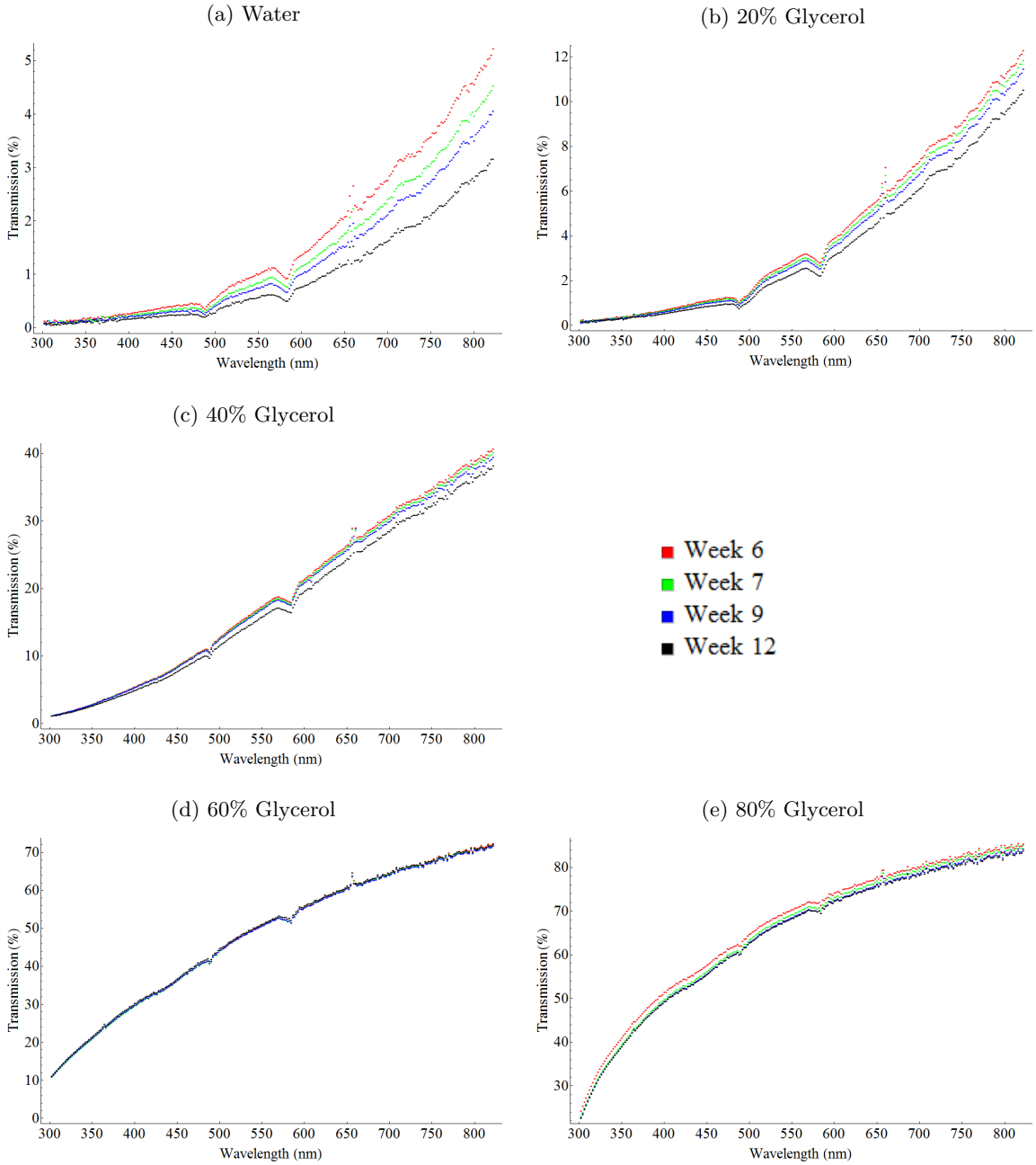

Figure 12: Spectroscopy measurements from week 6 onward

When looking at the later measurements shown in figure 12, they tell a different story. We see an increase in the turbidity, quite similar in nature for all mixtures, the only exception being figure 12d, which only shows very minor changes. Only the 60% and 80% sample have been centrifuged, and both at the same speed. It may be that because of this, some aggregation has occurred in the less viscous 60% sample which doesn't appear in the 80% sample. It seems to be stable.

The trend of increasing turbidity only appeared after the method of measurement was changed to keep using the same cuvettes over and over again, instead of using new ones every time. It is unlikely this is a coincidence. This suggests the varying results of figure 11 might have been caused by inhomogeneities throughout the bottle, or the method of pipetting the sample into the cuvettes may have sparked some aggregation, the one time more so than the other time.

Another possible explanation could be sedimentation. The light beam of the spectrometer passes through the lower part of the cuvette. Perhaps over time gravity caused the concentration of microfibrils in the bottom of the cuvette to increase. There was no visible sedimentation, however it cannot be ruled out.

What is apparent, however, is that something is happening in figure 12. This may be aggregation we're seeing, to look further into this, we will look at images of large scale structure made using confocal microscopy.

4.2.3 Confocal images of structure

Starting in week 3, images were made of the samples, as discussed in section 3.3.2. A milliliter of sample was dyed, which was then very thoroughly mixed.

A large number of images was taken, which is why it will only be possible to show a small selection of them. We'll be looking at the $750 \times 750\ \mu m^2$ images, because they give the best perspective of the structure.

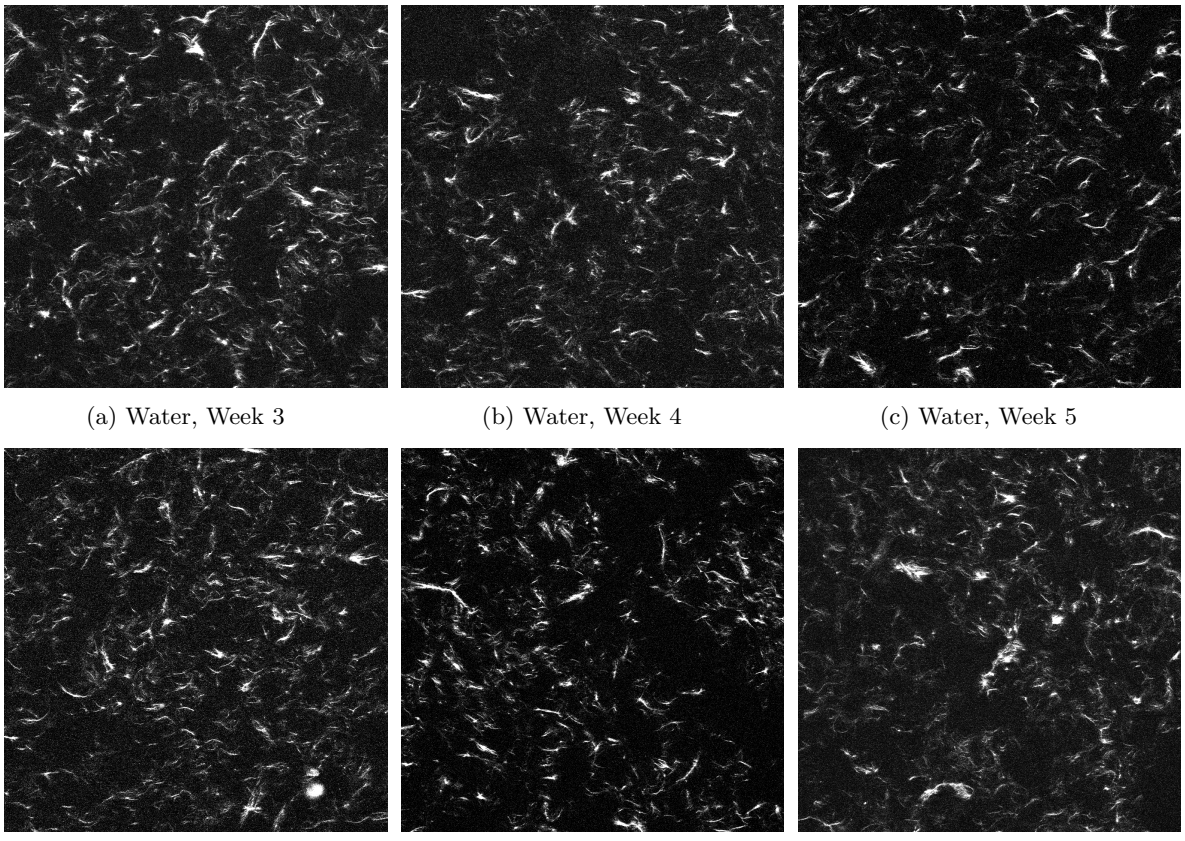

(a) Water, Week 3 (b) Water, Week 4 (c) Water, Week 5

(d) Water, Week 6 (e) Water, Week 7 (f) Water, Week 13

Figure 13: Confocal images (750 µm x 750 µm) of cellulose in water at different times, with enhanced contrast

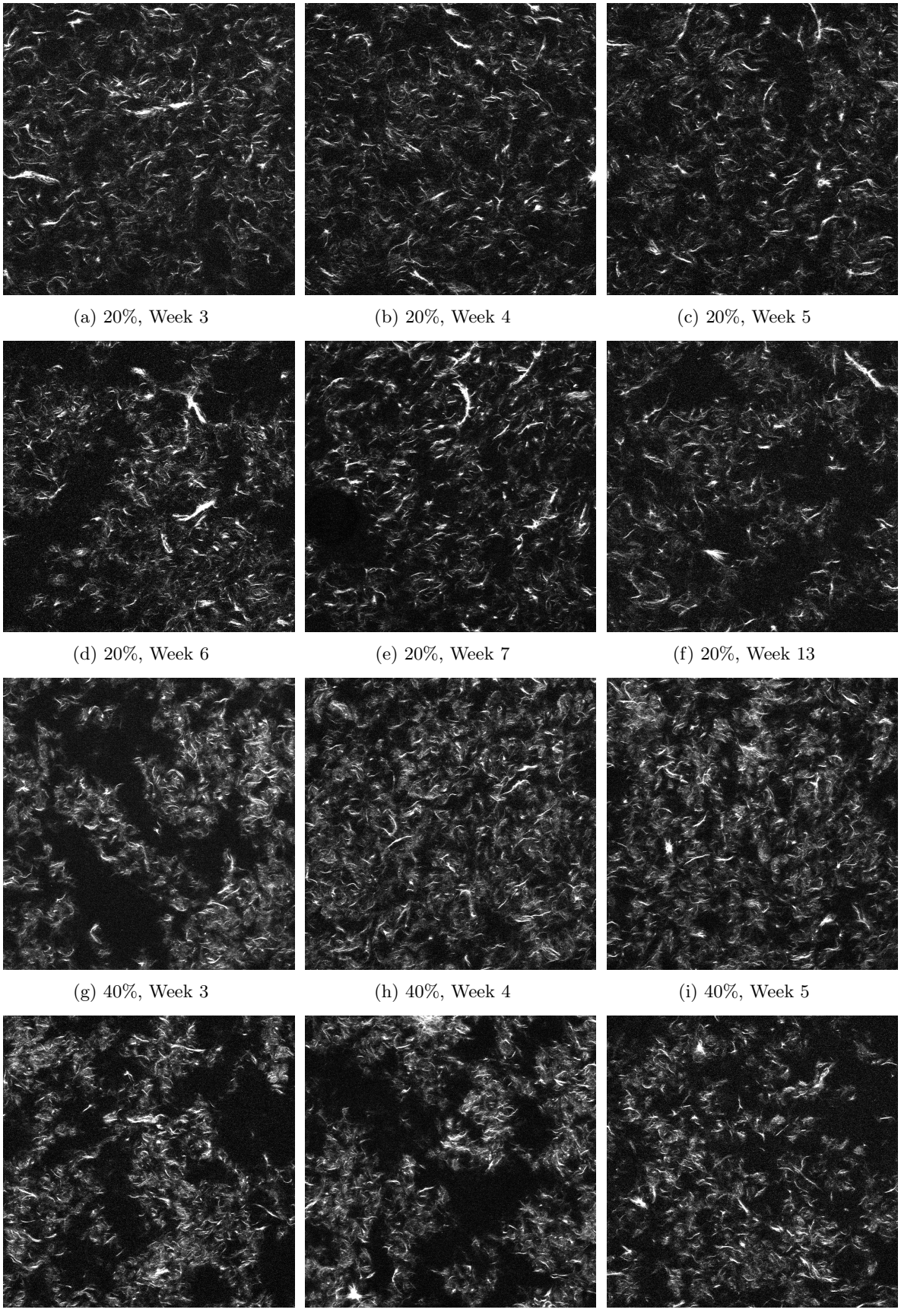

(a) 20%, Week 3 (b) 20%, Week 4 (c) 20%, Week 5

(d) 20%, Week 6 (e) 20%, Week 7 (f) 20%, Week 13

(g) 40%, Week 3 (h) 40%, Week 4 (i) 40%, Week 5

(j) 40%, Week 6 (k) 40%, Week 7 (l) 40%, Week 13

Figure 14: Confocal images (750 µm x 750 µm) of cellulose in 20% and 40% glycerol at different times, with enhanced contrast

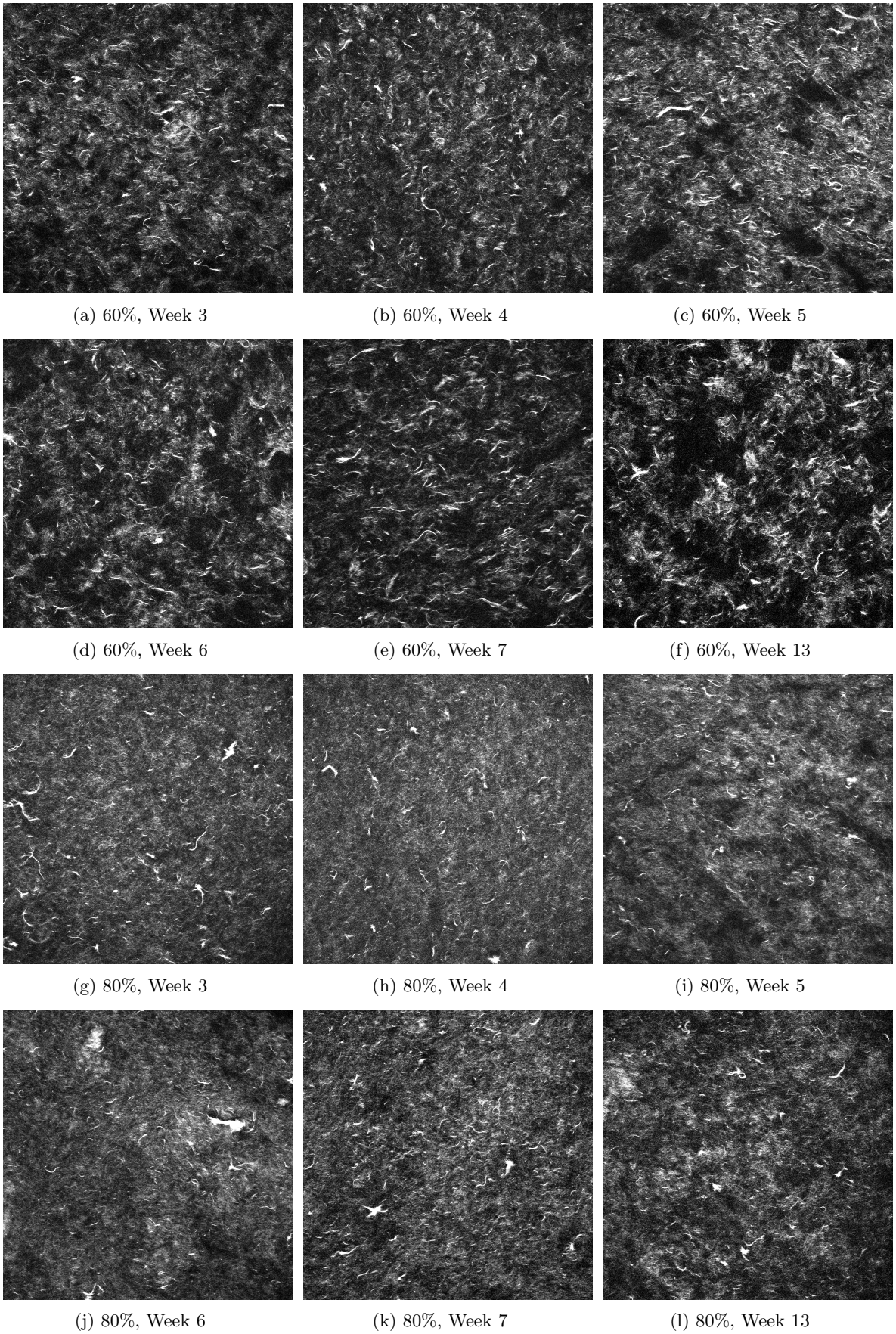

(a) 60%, Week 3 (b) 60%, Week 4 (c) 60%, Week 5

(d) 60%, Week 6 (e) 60%, Week 7 (f) 60%, Week 13

(g) 80%, Week 3 (h) 80%, Week 4 (i) 80%, Week 5

(j) 80%, Week 6 (k) 80%, Week 7 (l) 80%, Week 13

Figure 15: Confocal images (750 µm x 750 µm) of cellulose in 60% and 80% glycerol at different times, with enhanced contrast

There are five times as many images of size 750×750 μm^2. The images which were selected to be shown were chosen together as a set of six images, and not handpicked. Just looking at these images it is not very clear if there is an aggregating pattern hidden behind random fluctuations. The best cases for demonstrating the aggregation would be the 20% and 60% samples, where the voids between the flocks of cellulose seem to have increased in size, and the 40% sample shows a similar story if the image from the first week is excluded. A better understanding might be obtained by doing some further analysis with software such as ImageJ.

5 Conclusion and discussion

We have seen that by measuring the transmission spectrum, the dispersion relation for cellulose was determined, and found to match literature values reasonably well. Although the dispersion relation our measured values suggest has a different shape than the one found in literature, this can be explained as an effect of the vastly changing structure of the microfibril network over the different dispersions.

Over the course of several months, dispersions of cellulose microfibrils were imaged using confocal microscopy, and their transmission spectra were measured. Each of these experiments suggests a change in microstructure of the cellulose.
In the spectroscopy measurements an increased turbidity is found, which is to be expected when larger aggregates are being formed. However, the possibility this has been caused by sedimentation has not been excluded, although it is not seen as likely considering the second experiment.
In the images taken with the confocal microscope the structure of the network seems to have become more heterogeneous. This is difficult to quantify though, and further analysis would provide more certainty.
However, since we are seeing both effects simultaneously, it suggests the microfibrils are in fact aggregating due to van der Waals interactions over large time periods.

Acknowledgements

First and foremost I would like to thank my supervisors for helping me throughout this project, by setting out goals, helping me with theory and experiments, and nudging me in the right direction when I was stuck. Furthermore I would like to thank Jissy José for her help with confocal microscopy.
Finally, I would like to thank the Soft Condensed Matter group as a whole. I have found the work discussions and the weekly nanoseminar have broadened my horizon.

References

[1] J. Brandrup, E.H. Immergut, and E.A. Grulke. *Polymer Handbook*. Wiley, New York, 4th edition, 1999.

[2] J. D. Fontana, A. M. de Souza, C. K. Fontana, I. L. Torriani, J. C. Moreschi, B. J. Gallotti, S. J. de Souza, G. P. Narcisco andJ. A. Bichara, and L. F. X. Farah. Acetobacter cellulose pellicle as a temporary skin substitute. *Applied biochemistry and biotechnology*, 24/25:253, 1990.

[3] Robert D. Groot. Simulation of semiflexible chains. ii. fiber bundle networks. *The Journal of Chemical Physics*, 138:224904, 2013.

[4] Jacob Israelachvili. *Intermolecular & Surface Forces*. Elsevier Academic Press, San Diego, California, second edition, 1992.

[5] Marcus E. Carr Jr. and Jan Hermans. Size and density of fibrin fibers from turbidity. *Macromolecules*, 11:46–50, 1978.

[6] R. Malcolm Brown Jr. The biosynthesis of cellulose. *Journal of macromolecular science. Physics*, 33:1345–1373, 1996.

[7] Stefka N. Kasarova, Nina G. Sultanova, Christo D. Ivanov, and Ivan D. Nikolov. Analysis of the dispersion of optical plastic materials. *Optical Materials*, 29:1481–1890, 2006.

[8] A. Kuijk, R. Koppert, P. Versluis, G. van Dalen, C. Remijn, J. Hazekamp, J. Nijsse, and K.P. Velikov. Dispersions of attractive semiflexible fiberlike colloidal particles from bacterial cellulose microfibrils. *Langmuir*, 29:14356–14360, 2013.

[9] Glyn O. Philips, John F. Kennedy, and Peter A. Williams. *Cellulose: Structural and Functional Aspects*. Ellis Horwood Ltd, 1989.

[10] C. Yeromonahos, B. Polack, and F. Caton. Nanostructure of the fibrin clot. *Biophysical Journal*, 99:2018–2027, 2010.